

# Prediction of Soil Liquefaction Using Machine Learning Approaches

Md. Mahabub RAHMAN<sup>1</sup> , Md. Belal HOSSAIN<sup>1</sup> , Abu SAYED<sup>2</sup>\*)

<sup>1)</sup> *Department of Civil Engineering*

*Hajee Mohammad Danesh Science and Technology University*

Dinajpur, Bangladesh; e-mails: mmr.civil@hstu.ac.bd; mbh.civil@hstu.ac.bd

<sup>2)</sup> *Department of Civil Engineering, Pundra University of Science and Technology*

Gokul, Bangladesh

\*Corresponding Author e-mail: sayed55443138@gmail.com

In the geotechnical engineering field, the assessment of liquefaction potential is a critical aspect of site evaluation. This work focuses on the application of support vector machines (SVM) to improve the accuracy of liquefaction potential evaluation. Input data were collected from the authors' previous study and include parameters such as groundwater table (GWT), depth, fineness content, peak ground acceleration (PGA), corrected SPT-N value, total stress, and effective overburden stress. Radial basis function (RBF), linear, polynomial, and sigmoid are the four SVM kernel functions that are examined in this study to model liquefaction-related data using three approaches: grid search cross-validation,  $k$ -fold cross-validation, and fuzzy  $c$ -clustering means (FCM). Several performance metrics, including accuracy, precision, recall, and the area under the receiver operating characteristics (ROC) curve (AUC), among others, are used to evaluate the developed machine learning (ML) models. The linear and polynomial functions, for the grid search cross-validation approach, show higher performance with an accuracy of 94.64%, recall of 95.55%, F1-score of 96.63, and AUC of 0.99 on the testing data. For the  $k$ -fold partitioning approach, the RBF yields higher performance metrics compared to the other three functions, with an accuracy of 92.73%, precision of 100%, F1-score of 95.0%, and AUC of 0.98. In the FCM technique, the linear and polynomial kernels again yield greater accuracy, precision, F1-score, and specificity, while, the AUC values of the sigmoid and RBF kernels are higher. The current analysis recommends the RBF over other mathematical functions based on the  $k$ -fold partitioning technique after evaluating all performance matrices.

**Keywords:** liquefaction; support vector machine; mathematical functions; divisional approaches; performance metrics.



Copyright © 2025 The Author(s).

Published by IPPT PAN. This work is licensed under the Creative Commons Attribution License CC BY 4.0 (<https://creativecommons.org/licenses/by/4.0/>).

## 1. INTRODUCTION

In the design phase of civil engineering construction, assessing the potential for soil liquefaction due to earthquakes is a critical concern [1]. This is because

ground failure may occur when an earthquake causes the soil layer underneath the buildings to liquefy. Eventually, this results in severe structural damage or even collapse. Liquefaction is the term for the solid-to-liquid transition in granular materials that can be triggered by an increase in pore water pressure [2]. Several conditions can lead to soil liquefaction hazards: (1) loose and non-cohesive soil particles; (2) soil particle sizes ranging from small grains of sand to granular silt; (3) sufficient ground shaking from an earthquake; and (4) a saturated soil state [3]. In the early development of soil mechanics, TERZAGHI and PECK (1948) identified the soil liquefaction phenomenon to explain the loss of strength in saturated, loose, granular soil deposits [4]. Several studies have examined liquefaction and the resulting ground failures resulting from seismic activity, including the 1964 Alaskan and Niigata earthquakes, which led to the collapse of foundations, bridges, and slopes. Significant damage to structures and infrastructure has been inflicted by historical earthquakes in Bangladesh and Northeast India, including the Great Indian Earthquake of 1897, the Bengal Earthquake of 1885, and the Srimangal Earthquake of 1918 [5]. Due to the presence of active faults and tectonic plate boundaries, this region is highly susceptible to earthquakes with magnitudes ranging from moderate to high [6]. In developing countries, such seismic events can result in high death tolls and extensive damage to industrial zones, ports, and construction infrastructure. Soil liquefaction is one of the primary contributors to this increased vulnerability [7].

Liquefaction caused by earthquakes has been reported and assessed in numerous parts of the world. SEED and IDRISS [8] proposed one of the earliest and most fundamental procedures for determining soil liquefaction potential. Their semi-empirical technique estimates a site's liquefaction resistance using results from the in-situ standard penetration test (SPT). This semi-empirical technique relies on the findings of the on-site standard penetration test (SPT) to determine the site's liquefaction susceptibility. To assess soil liquefaction in the field, later techniques, based on shear wave velocity ( $V_s$ ) and the cone penetration test (CPT), were presented in [9, 10]. Since 1971, liquefaction prediction has used SPT, CPT, and  $V_s$  as the accepted methods. These techniques, however, introduce a great deal of uncertainty since they use "limit states", which are determined based on engineering judgment, to distinguish between liquefaction and non-liquefaction scenarios. Recent research has demonstrated that ML techniques can be used to build the "limit state" in a more logical manner. Unlike traditional approaches (e.g., empirical, experimental), ML-based algorithms for prediction have advanced rapidly in recent decades, providing a new way to address geotechnical issues due to their high nonlinear fitting capabilities. Indeed, ML algorithms have been widely employed in geotechnical engineering to forecast soil shear strength [11], soil consolidation coefficient [12], piling capacity [13], and slope stability [14].

Additionally, algorithms based on ML have been used to forecast soil liquefaction. For instance, NAJJAR and ALI [15] used CPT data in a ML framework to examine soil liquefaction. Their artificial neural network (ANN) models developed using input parameters such as water content, plasticity index, and liquid limit, demonstrated a reliable and conventional prediction rate for evaluating liquefaction potential. KURUP and GARG [16] used artificial neural networks, considered unconventional at the time, which proved to be trustworthy tools for assessing liquefaction potential. In other studies, seismic liquefaction susceptibility was effectively assessed using support vector machines (SVM) and relevance vector machines (RVM) [17, 18]. HANNA *et al.* [19] developed a neural network model, an alternative to general regression model, to establish relationships between 12 soil characteristics and seismic data, enabling reliable prediction of liquefaction occurrence. RAHMAN *et al.* [20] also employed ANN, which is very useful for handling large datasets. Their ANN model achieved accuracy levels comparable to earlier studies that employed a large number of parameters. KOHESTANI *et al.* [21] described a random forest (RF) technique to assess the probability of earthquake-induced soil liquefaction. Their findings showed that the RF models outperformed both ANN and SVM models in terms of accuracy. In a separate study, the performance of the stochastic gradient boosting (SGB) approach was examined using both SPT and CPT data [22]. The SPT test data set was found to have the highest classification accuracy. Multi-objective feature selection (MOFS) methods were employed by DAS *et al.* [23] to predict liquefaction susceptibility using shear wave velocity ( $V_s$ ), CPT, and SPT data. It was discovered that the CPT-based models outperformed those based on SPT and  $V_s$  in terms of efficiency. Four ML algorithms – K2, Hill Climbing, Tree Augmented Naive, and Tabu Search – were employed by AHMAD *et al.* [24] to evaluate the soil liquefaction based on CPT data. The most critical parameters for prediction accuracy were found to be vertical effective stress and cone tip resistance. HU [25] developed two different Bayesian network (BN) models using dynamic penetration test (DPT) and shear wave velocity test data. These two models were validated against other existing models, and demonstrated better predictive performance. Finally, several international studies have examined the viability of ML methods for seismic liquefaction evaluation using SPT and CPT data. These studies emphasize the significance of selecting relevant input factors, using large datasets, and addressing the shortcomings of both traditional and current ML-based models [26–30].

This article’s aim is to examine the feasibility of four different mathematical functions of support vectors (RBF, linear, polynomial, and sigmoid) using three approaches: grid search cross-validation, FCM, and  $k$ -fold cross-validation. Seven input parameters were selected from the authors’ previous research, which assessed soil liquefaction utilizing empirical approaches based on SPT data [31, 32].

To examine the capabilities of the proposed model in estimating liquefaction potential, several statistical performance parameters were examined. In order to assess the proposed model’s predictive power for soil liquefaction vulnerability, several statistical factors were examined.

## 2. MATERIALS AND METHODS

### 2.1. Study area and dataset

The dataset used in this study was obtained from a previous study that assessed seismic soil liquefaction using field data from SPTs. The entire city of Dinajpur, Bangladesh, was covered by the borehole log data used in the previous study. Four different patterns were identified in the surface geology of the study area. The old gravelly sand and the Barind clay residue extend across the district’s northern section. To the north of the district lies a young, gravelly sand desert. The majority of the southeast and south of the area is covered by Barind clay residue, along with alluvial silt and young gravelly sand. A significant portion of the study area was found to be at risk of liquefaction due to the presence of cohesionless soil at shallow depths. Figure 1 shows the dataset, which contains 199 instances classified as liquefiable and 78 instances classified as non-liquefiable [31, 32].

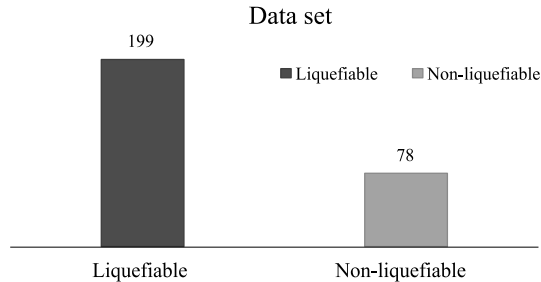


FIG. 1. Bar chart of liquefiable and non-liquefiable cases.

Seven influencing factors were selected as input parameters, including soil layer depth ( $Z$ ), total overburden stress ( $\sigma_{av}$ ), effective stress ( $\sigma'_{av}$ ), fines content ( $F$ ), corrected SPT-N ( $N_{1(60cs)}$ ), GWT, and PGA. Table 1 shows the descriptive statistics of the input dataset used for this study.

### 2.2. Nonlinear separable SVM

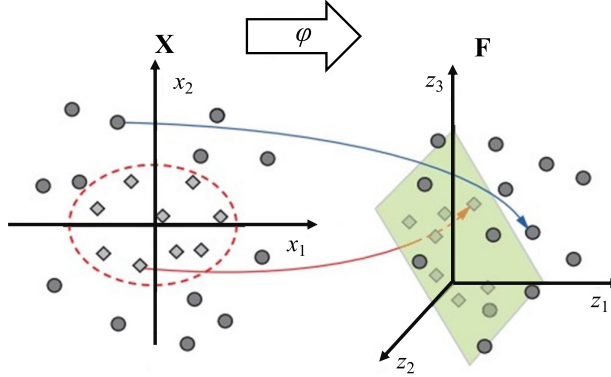
When the input space is mapped onto a high-dimensional space  $x \rightarrow f(x)$ , a nonlinear separation hyperplane is created, where the data can be classified linearly (Fig. 2). This mapping’s key characteristic is that the function has to

TABLE 1. Descriptive statistical information of the input dataset.

	$Z$	$N_{1(60cs)}$	$F < 0.0075$	GWT	$\sigma_{av}$	$\sigma'_{av}$	PGA
Mean	3.73987	11.2083	75.640072	2.5713	68.4324	45.2945	0.21827
Std. dev.	2.53335	6.06883	22.093035	0.72395	46.3925	22.5195	0.47312
Min	0.7621	2.2921	11	1.5	18.2427	1.1043	0.03
25%	1.82	7.6014	62	2.25	30.2796	27.8089	0.14
50%	3.81	10.1377	84	2.5	63.0831	40.5989	0.21
75%	5.33	13.9004	95	3	91.8521	54.3878	0.23
Max	10.67	70.1165	99	4.75	199.15	115.35	8

satisfy the requirement that it can be expressed as a kernel function  $K(x_i, x_j)$  for the dot product of the two functions,  $f(x_i) \cdot f(x_j)$ . Then, the decision function becomes Eq. (2.1).

$$(2.1) \quad f(x) = \sum y_i \alpha_i K(x_i, x_j) + b.$$


 FIG. 2. Mapping from the data space  $X$  to the feature space  $F$ .

Diverse learning machines can be built using different kernel functions. Equations (2.2) and (2.3) are examples of commonly used kernel functions:

$$(2.2) \quad \begin{cases} \text{linear kernel: } K(x_i, x_j) = [x_i]^T [x_j], \\ \text{polynomial kernel: } K(x_i, x_j) = (Y [x_i]^T [x_j] + r)^r, \quad Y > 0, \\ \text{radial basis function (RBF): } K(x_i, x_j) = \exp(-Y \|x_i - x_j\|^2 / 2), \quad Y > 0, \end{cases}$$

and

$$(2.3) \quad \text{sigmoid kernel: } K(x_i, x_j) = \tan(Y [x_i]^T [x_j] + r).$$

### 2.3. Methodology

The Scikit-Learn library, implemented in the Python programming language, was used for ML models, and the corresponding codes were developed for performance evaluation in this study. Figure 3 illustrates the complete workflow for this study.

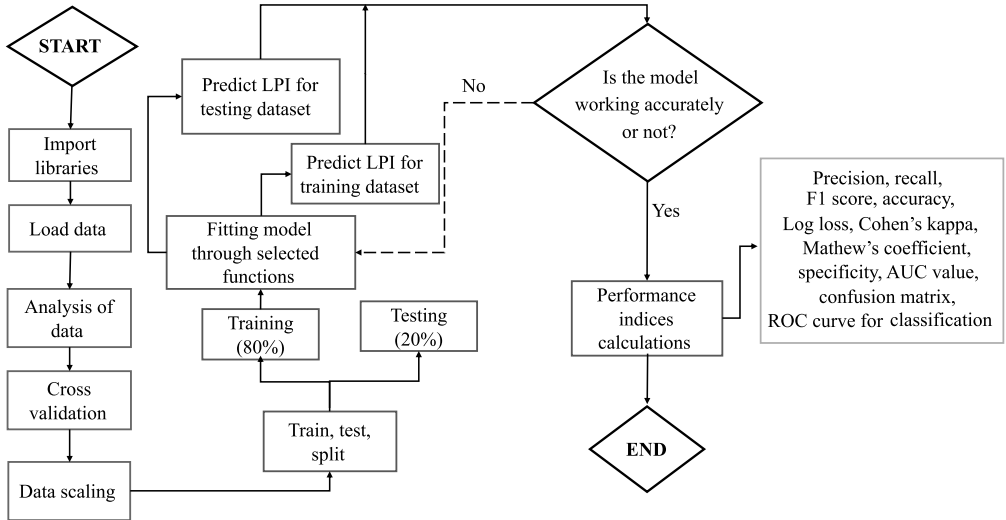


FIG. 3. Flow chart of the research methodology.

*2.3.1. GridSearch cross-validation.* Hyperparameter tuning is a procedure that GridSearch cross-validation (GridSearchCV) uses to find the best values for a particular model (Fig. 4). As was already said, a model's performance

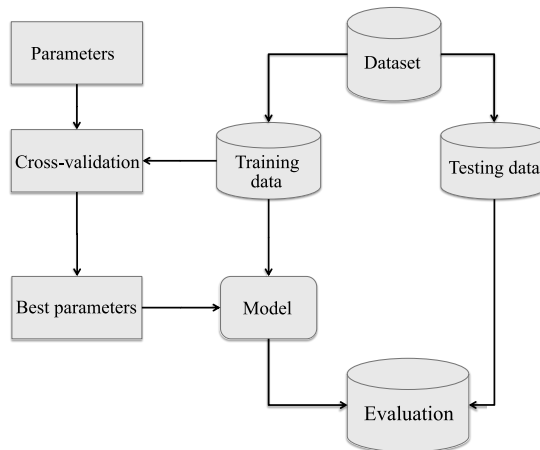


FIG. 4. Working procedure of GridSearchCV.

is greatly influenced by the values of its hyperparameters. The best values for hyperparameters cannot be determined in advance; therefore, it is recommended to try every conceivable value before determining the ideal values. GridSearchCV is usually used to automate the hyperparameter tuning process, as performing it by hand could require a significant amount of time and resources.

*2.3.2. The  $k$ -fold division approach.* The  $k$ -fold partitioning approach's data-splitting procedure is shown in Fig. 5. The  $k$ -fold method uses random shuffling to split the dataset into  $k$  folds. After  $k$ -fold splits the dataset, the first fold is used as the testing dataset, and the subsequent  $k - 1$  folds are used to create the training set. The model is trained with certain hyperparameters using the training data ( $k - 1$  folds) and the testing data from a single fold. The performance of the model is recorded. This process is repeated until all  $k$ -folds have been tested. The complete dataset is divided into training and testing using fivefold cross-validation.

*2.3.3. FCM approach.* Clustering is the process of grouping a dataset into subsets. Observations that are similar to one another are represented by each group, while items that are not comparable to one another are placed into distinct groups. In fuzzy clustering, an observation may belong to multiple clusters based on its membership value. For each observation distributed across the clusters, the total membership value is 1.0. SHI [33], SHAHIN *et al.* [34], and DAS [35] provide some background material on this methodology.

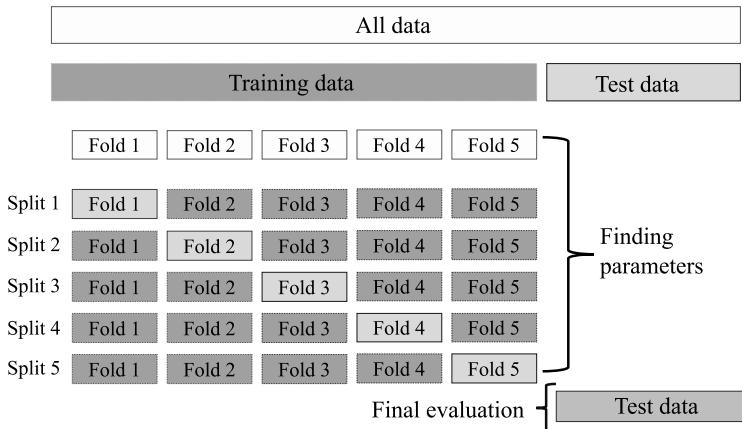


FIG. 5. Data splitting process in the  $k$ -fold cross-validation approach [36].

*2.3.4. Performance evaluation.* The confusion matrix is a commonly used tool in binary classification problems [37]. Table 2 illustrates the four compo-

TABLE 2. Components of the confusion matrix.

		Predicted label	
		Negative	Positive
Actual label	Negative	TN	FP
	Positive	FN	TP

nents of a confusion matrix: true positive (TP), false positive (FP), true negative (TN), and false negative (FN).

Based on the confusion matrix, the following performance measures can be calculated:

- (i) accuracy

$$(2.4) \quad \text{ACC} = \frac{\text{TP} + \text{TN}}{\text{TP} + \text{TN} + \text{FP} + \text{FN}},$$

- (ii) precision (P), recall (R) and F1-score (F1). The F1-score is used to evaluate a classification model's prediction accuracy by combining the precision and recall. Here is how these measurements are computed:

$$(2.5) \quad \left\{ \begin{array}{l} P = \frac{\text{TP}}{\text{TP} + \text{FP}}, \\ R = \frac{\text{TP}}{\text{TP} + \text{FN}}, \\ \text{F1} = \frac{2 \cdot P \cdot R}{P + R}, \end{array} \right.$$

- (iii) Cohen's kappa ( $K$ ). It takes into account the chance of an unintentional agreement [38]. The definition of Cohen's kappa is as follows:

$$(2.6) \quad K = \frac{P_0 - P_e}{1 - P_e},$$

where  $P_e$  is the probability expected by chance and  $P_0$  is the complete agreement probability, which is equal to the accuracy.

- (iv) Matthew's correlation coefficient (MCC). This is a statistical metric used to assess how well binary classification models perform, especially in cases involving unbalanced datasets. It considers false positives, false negatives, true positives, and true negatives.
- (v) Area under the curve (AUC) and receiver operating characteristic (ROC). These two are frequently employed in binary classification to assess classification accuracy [39]. The ROC curve is generated by plotting the true

positive rate (TPR) on the vertical axis against the false positive rate (FPR) on the horizontal axis across various threshold settings. The top-left corner represents the “ideal” location, where  $FPR = 0$  and  $TPR = 1$ . Consequently, a larger AUC indicates better classification accuracy. Table 3 shows the hyperparameters used for each mathematical function.

TABLE 3. Hyperparameters used for each mathematical function.

Approach	Hyperparameters			
	RBF	Linear	Polynomial	Sigmoid
GridSearch	$C = 1000,$ $\gamma = 0.01$	$C = 100,$ $\gamma = 0.01$	$C = 1000,$ $\text{coef0} = 1.0,$ $\text{degree} = 2,$ $\gamma = 0.01$	$C = 100,$ $\text{coef0} = 0.1,$ $\text{degree} = 2,$ $\gamma = 0.01$
$k$ -fold	$C = 1000,$ $\gamma = \text{scale}$	$C = 1000,$ $\gamma = 0.01$	$C = 1000,$ $\text{coef0} = 1.0,$ $\text{degree} = 2,$ $\gamma = 0.01$	$C = 100,$ $\text{coef0} = 0.1,$ $\text{degree} = 5,$ $\gamma = 0.01$
FCM	$C = 1000,$ $\gamma = \text{scale}$	$C = 1000,$ $\gamma = 0.01$	$C = 1000,$ $\text{coef0} = 1.0,$ $\text{degree} = 2,$ $\gamma = 0.01$	$C = 100,$ $\text{coef0} = 0.1,$ $\text{degree} = 5,$ $\gamma = 0.0001$

To develop specific models, the dataset was trained with five fold cross-validation for GridSearchCV and the  $k$ -fold approach. The number of clusters for FCM approach was set to 5. The average value of the cross-validation results was calculated and then sorted based on different parameters using the GridSearch technique. Next, these optimized results were used for further model tuning in both  $k$ -fold and FCM approaches.

### 3. RESULTS AND DISCUSSION

This investigation developed three models, each based on different approaches, to meet the research objectives. Table 3 provides the value ranges for the parameters used and the total number of experiments for each algorithm. The models were developed using the best parameters obtained through cross-validation in the case of the GridSearch technique. However, in the case of the  $k$ -fold and FCM methods, the best parameters were selected based on the trial-and-error method, based on the resulting accuracy in predicting the target variable. The best combinations obtained for each mathematical function, including RBF, linear, polynomial, and sigmoid, are given in Table 3. These best parameter combinations, as specified in Table 3, were then applied to the entire dataset and incorporated into the study’s outputs. Some hyperparameter combinations

produced identical results, and one of these combinations is presented in summary. The models were developed using the best parameters obtained through cross-validation as well as the mentioned parameters for the  $k$ -fold and FCM approaches.

As stated before, the hyperparameters for this study were tuned using the GridSearchCV technique (Model I), and then the  $k$ -fold cross-validation technique was used for the train-test split to develop Model II. Finally, the fuzzy clustering approach was used to find the best model for predicting soil liquefaction in this study. The number of support vectors is important because it reveals information about the SVM model's complexity and its capacity to generalize to new, untested data. Generally, a simpler decision boundary with fewer support vectors may be more reliable and less prone to overfitting. Conversely, a higher number of support vectors may indicate a more complex decision boundary, potentially leading to overfitting the training data. Figure 6 shows the number of support vectors for each approach with each mathematical function.

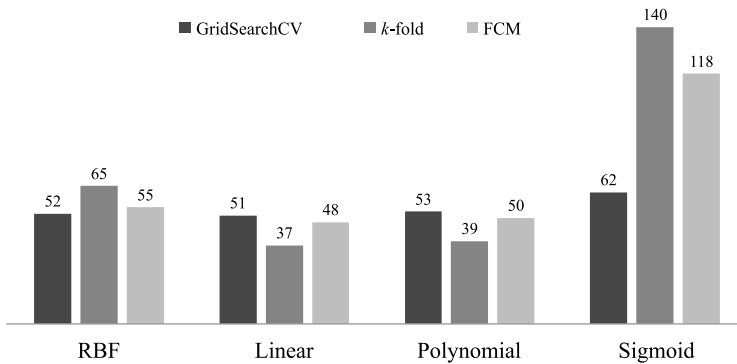


FIG. 6. Number of support vectors.

It is clear from the figure that the different kernels and techniques result in varying numbers of support vectors. When considering the RBF, polynomial, and sigmoid kernels, fewer support vectors are typically found for linear kernels. In both the  $k$ -fold and FCM techniques, the sigmoid kernel has a comparatively larger number of support vectors. In all approaches, the RBF kernel shows a moderate number of support vectors. A lower count of support vectors may indicate a more straightforward model that is more likely to generalize well to new data. A higher count could suggest a more sophisticated model, which is prone to overfitting. A confusion matrix is a statistical tool used to evaluate the performance of classification algorithms, particularly useful for binary classification problems with only two possible classes, such as the one in this study. The confusion matrices for Model I, Model II, and Model III are represented in Figs. 7–10, Figs. 11–14, and Figs. 15–18, respectively.

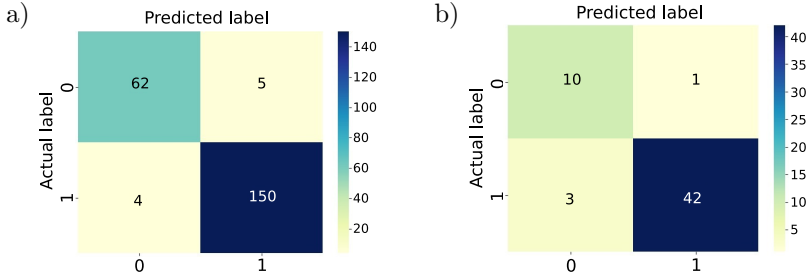


FIG. 7. Confusion matrix for GridSearchCV (Model I) with RBF mathematical function: a) training and b) testing.

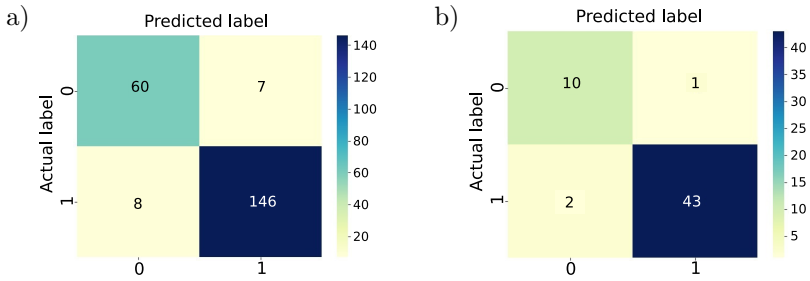


FIG. 8. Confusion matrix for GridSearchCV (Model I) with linear mathematical function: a) training and b) testing.

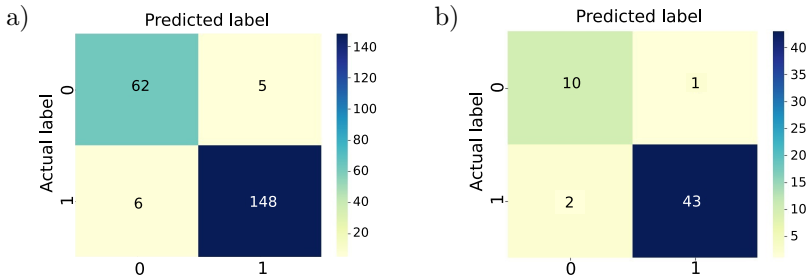


FIG. 9. Confusion matrix for GridSearchCV (Model I) with polynomial mathematical function: a) training and b) testing.

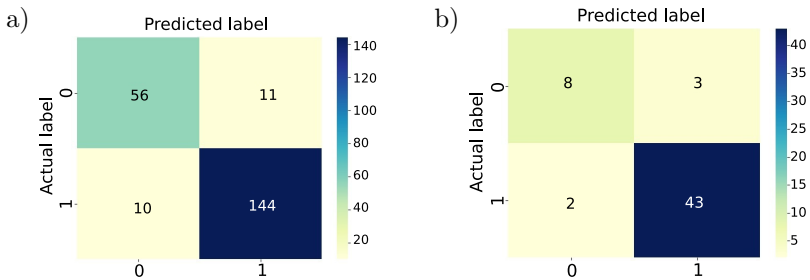


FIG. 10. Confusion matrix for GridSearchCV (Model I) with sigmoid mathematical function: a) training and b) testing.

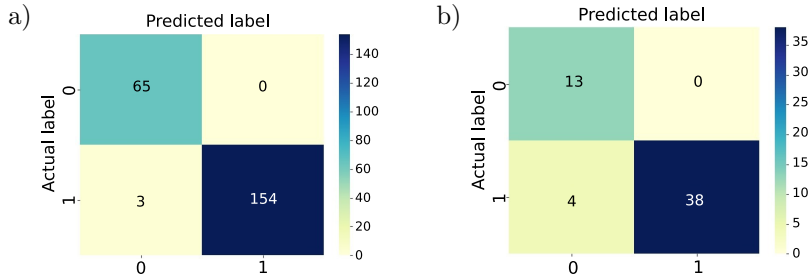


FIG. 11. Confusion matrix for the  $k$ -fold partitioning approach (Model II) with RBF mathematical function: a) training and b) testing.

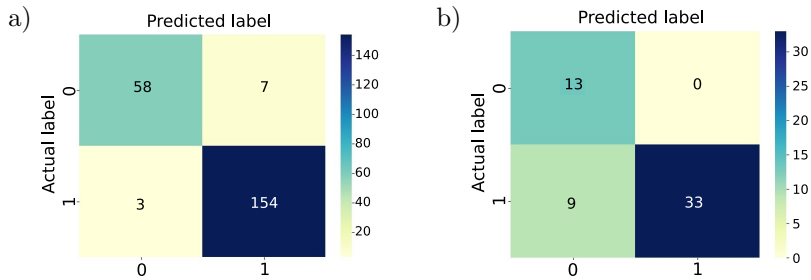


FIG. 12. Confusion matrix for the  $k$ -fold partitioning approach (Model II) with linear mathematical function: a) training and b) testing.

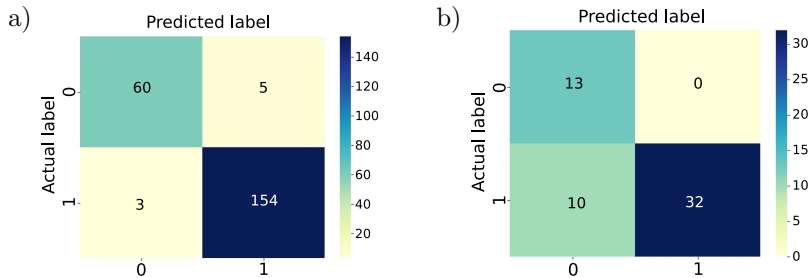


FIG. 13. Confusion matrix for the  $k$ -fold partitioning approach (Model II) with polynomial mathematical function: a) training and b) testing.

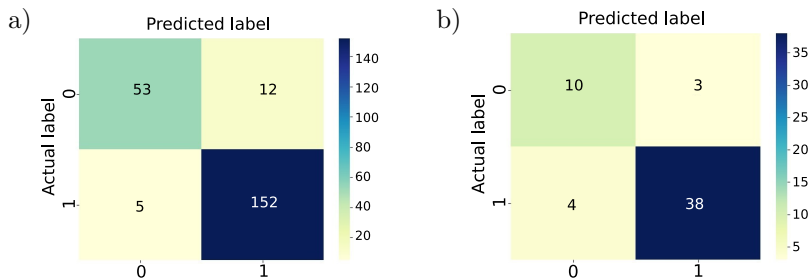


FIG. 14. Confusion matrix for the  $k$ -fold partitioning approach (Model II) with sigmoid mathematical function: a) training and b) testing.

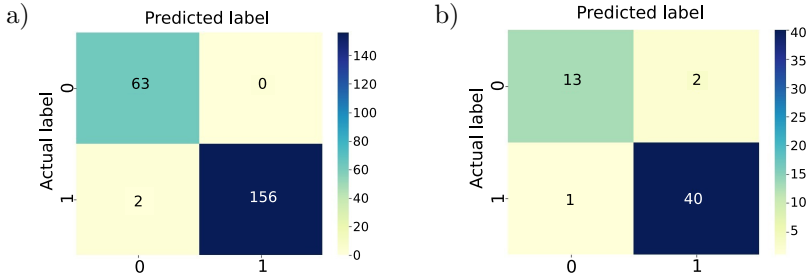


FIG. 15. Confusion matrix for the FCM clustering approach (Model III) with RBF mathematical function: a) training and b) testing.

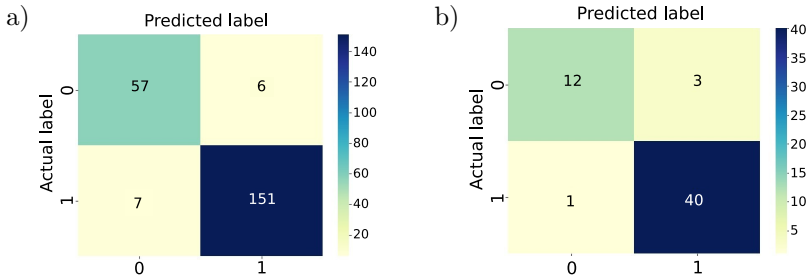


FIG. 16. Confusion matrix for the FCM clustering approach (Model III) with linear mathematical function: a) training and b) testing.

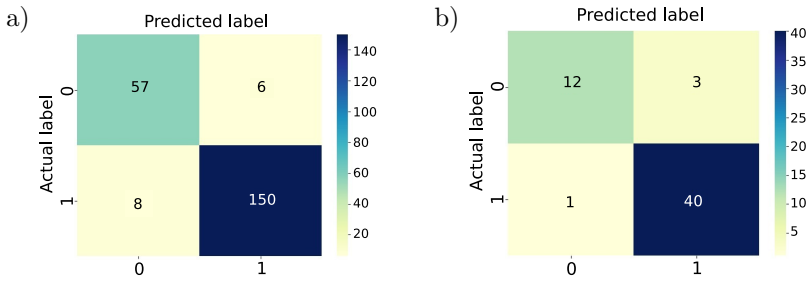


FIG. 17. Confusion matrix for the FCM clustering approach (Model III) with polynomial mathematical function: a) training and b) testing.

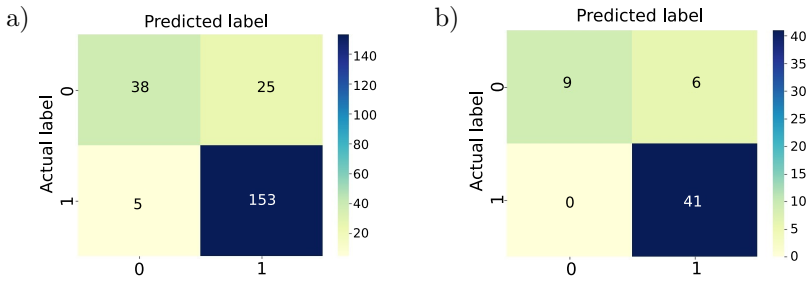


FIG. 18. Confusion matrix for the FCM clustering approach (Model III) with sigmoid mathematical function: a) training and b) testing.

TABLE 4. Comparison of the performance of the three developed models.

Performance metrics		GridSearchCV (Model I)			<i>k</i> -fold CV (Model II)			FCM approach (Model III)					
		RBF	Linear	Polynomial	Sigmoid	RBF	Linear	Polynomial	Sigmoid	RBF	Linear	Polynomial	Sigmoid
Accuracy	Training	95.92	93.21	95.02	90.49	98.64	95.49	96.39	92.34	97.77	92.76	92.76	88.23
	Testing	92.85	94.64	94.64	91.07	92.73	83.64	81.82	87.27	91.07	92.85	92.85	87.50
Precision	Training	96.77	95.42	96.73	92.90	1.00	95.65	96.85	92.68	99.35	95.51	95.51	95.51
	Testing	97.67	97.73	97.73	93.48	1.00	1.00	1.00	92.68	89.13	93.02	93.02	85.42
Recall	Training	97.40	94.81	96.10	93.51	98.08	98.08	98.08	96.81	97.46	94.30	94.30	94.30
	Testing	93.33	95.55	95.55	95.55	90.48	78.57	76.19	90.47	1.00	97.56	97.56	1.00
F1-score	Training	97.08	95.11	96.42	93.20	99.03	96.85	97.46	94.70	98.40	94.90	94.90	94.90
	Testing	95.45	96.63	96.63	94.50	95.00	88.00	86.48	91.56	94.25	95.24	95.24	92.13
Kappa	Training	90.32	84.00	88.27	77.41	96.78	88.92	94.22	80.91	94.25	92.41	82.46	82.41
	Testing	78.82	83.59	83.59	70.71	81.78	63.41	60.26	65.65	74.54	80.94	80.98	62.59
MCC	Training	90.32	84.01	88.27	77.42	96.83	89.01	94.22	81.15	94.57	82.43	82.43	82.43
	Testing	79.27	83.72	83.72	70.83	83.18	68.18	65.62	65.65	77.08	81.35	81.35	67.49
Specificity	Training	92.54	89.55	92.54	83.58	1.00	89.23	92.31	81.53	98.41	88.89	88.89	68.25
	Testing	90.91	90.91	90.91	72.73	1.00	1.00	1.00	76.92	66.67	80.00	80.00	53.33

The confusion matrix for Model I is presented for four mathematical functions. Among them, the linear and polynomial functions give the best accuracy. Both models correctly predicted 53 out of 56 instances in the testing data-set (Figs. 8 and 9). However, the other two mathematical functions correctly predicted 51 occurrences. For Model II, Fig. 11 shows that the RBF mathematical function provides more accurate results than the other three. For the testing data, the RBF function correctly predicted 51 out of 55 instances. However, the polynomial, linear, and sigmoid functions correctly predicted 45, 46, and 48 occurrences, respectively. Lastly, the best accuracy for Model III is provided by the linear and polynomial functions, just like in Model I. Both mathematical functions accurately predicted 52 out of 56 instances, as shown in Figs. 16 and 17. Nonetheless, the sigmoid function and RBF accurately predicted 49 and 51 instances, respectively. The performance metrics for the four mathematical functions of the three models are compiled in Table 4. These outcomes are the results of the model's subsequent attempts on the 20% test set, which was randomly chosen using the cross-validation procedure, with GridSearchCV yielding the best results.

Table 4 shows that Model I achieves its highest accuracy for the linear and polynomial functions, with 94.64% for testing and 95.92% for RBF in the training dataset. The outcomes for the testing dataset are more significant in a classification model and are higher for the linear and polynomial functions. In comparison to the linear function, the polynomial function exhibits a better accuracy score (95.02%) for the training data. Other performance measures for the testing data, including accuracy (94.64), recall (95.55%), F1-score (96.63%), kappa coefficient (83.59%), MCC (83.72%), and specificity (90.91%), are higher for the linear and polynomial functions in Model I, as shown in Table 4. Similarly, when the dataset is tested using the  $k$ -fold cross-validation approach, the best model, based on the confusion matrix, is obtained for the RBF function, which correctly predicted 51 out of 55 instances (Fig. 11). The other performance metrics in Table 4 indicate that the best-developed model is the RBF function, with accuracy (98.64%, 92.73%), precision (100%, 100%), recall (98.08%, 90.48%), F1-score (99.03%, 95.0%), kappa coefficient (96.78%, 81.78%), MCC (96.83%, 83.18%), and specificity (100%, 100%) for training and testing, respectively. Finally, in the case of the FCM approach, the confusion matrix for the linear and polynomial functions depicts the same results for both the testing (52 instances correctly predicted out of 56) and training (205 instances accurately predicted out of 221) data (Figs. 16 and 17). The summary in Table 4 for the FCM approach shows that the linear and polynomial functions yield the same results, including accuracy (92.76%, 92.85%), precision (95.51%, 93.02%), recall (94.3%, 97.56%), F1-score (94.9%, 95.24%), kappa coefficient (92.41%, 80.94%), MCC (82.43%, 81.35%), and specificity (88.89%, 80.0%) for training and testing, respectively.

This investigation also evaluates the ROC performance indicator, which plots the true positive rate on the  $y$ -axis and the false positive rate on the  $x$ -axis. The upper left corner of the plot represents the “ideal” location, where the true positive rate is 1 and the false positive rate is 0 [40]. In other words, the true positive rate is the proportion of liquefied soils that the model correctly identified as liquefied. On the other hand, the false positive rate refers to the proportion of non-liquefied soils that the model incorrectly predicted as liquefied. Figures 19, 20, and 21 present the ROC curves along with the AUC values for Models I, II, and III, respectively.

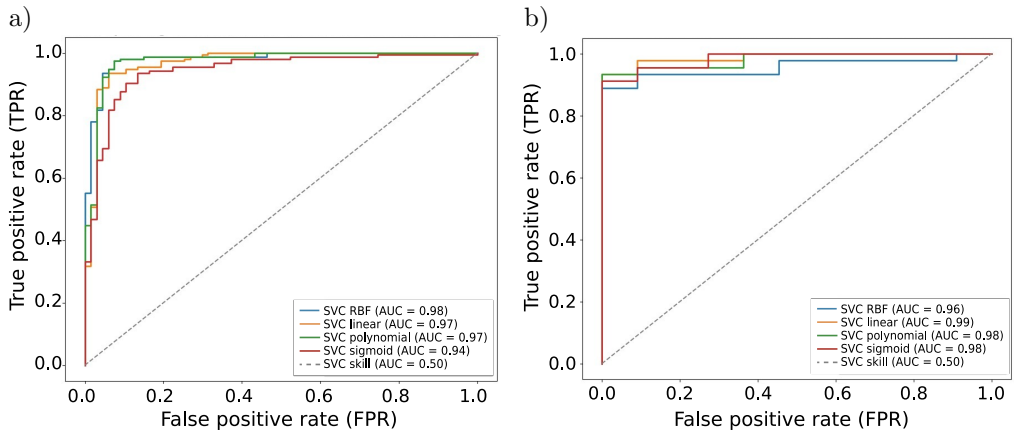


FIG. 19. ROC curve with AUC value for GridSearchCV (Model I) for: a) training and b) testing.

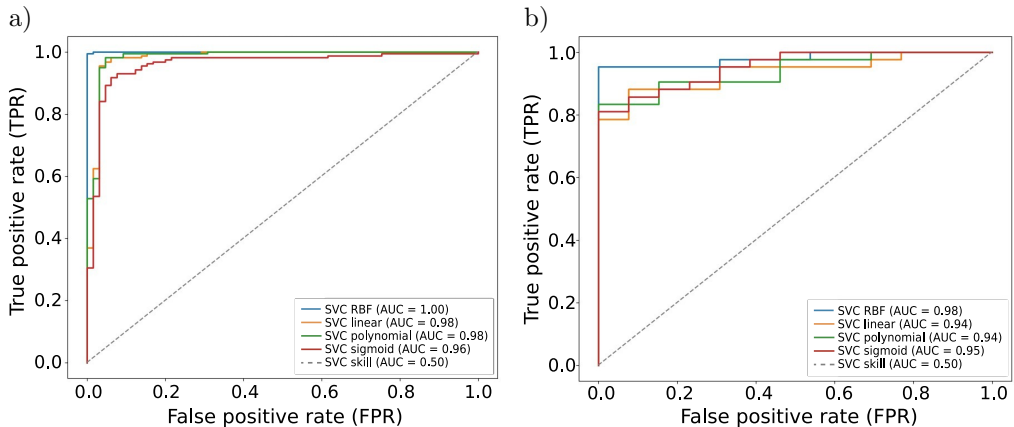


FIG. 20. ROC curve with AUC value for  $k$ -fold (Model II) for: a) training and b) testing.

For the testing data, the linear (AUC = 0.99) and polynomial (AUC = 0.99) functions yield the maximum AUC value for the GridSearch approach. The linear

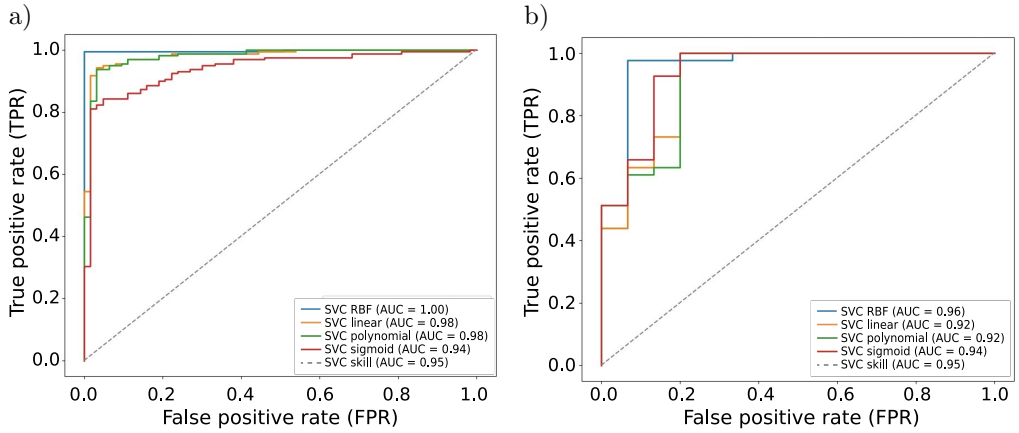


FIG. 21. ROC curve with AUC value for FCM (Model III) for:  
a) training and b) testing.

(AUC = 0.97) and polynomial (AUC = 0.97) are also acceptable, although the maximum AUC for the training data is achieved with the RBF function (AUC = 0.98). For the  $k$ -fold cross-validation, the RBF function achieves an AUC of 1.0 for training data and a higher AUC of 0.98 for testing data. In contrast, for the FCM technique the RBF function has the greatest AUC compared to linear and polynomial functions, with AUC = 0.89 for both training and testing data, compared to linear and polynomial functions, which have AUC = 1.0 for training and AUC = 0.97 for testing data.

#### 4. CONCLUSIONS

This study employed a well-known ML technique called support vector classification, employing four mathematical functions to create three models for predicting soil liquefaction. The developed models are capable of estimating the likelihood of liquefaction in all possible scenarios. As previously stated, this study evaluated the applicability of FCM,  $k$ -fold, and GridSearchCV techniques in liquefaction prediction. The best-performing models for predicting soil liquefaction were selected based on the confusion matrix, ROC performance indicator, and seven other performance metrics. For Model I, the linear and polynomial functions yield the highest accuracy (94.64%) for testing; however, the RBF function yields the highest accuracy (98.64%) for training and 92.73% for testing in the  $k$ -fold partitioning approach. As with Model I, the polynomial and linear functions yield the best performance metrics for the FCM clustering approach, with accuracy of 92.76% for training and 92.85% for testing. The confusion matrix and ROC performance indicator validate these results.

Out of the models developed using three different methods and four different mathematical functions, the RBF is the best model for the  $k$ -fold cross-validation because its performance metrics (precision = 100%, recall = 90.48%, F1-score = 95.0%, kappa coefficient = 81.78%, MCC = 83.18%, specificity = 100%, and AUC = 0.98 for testing) align most closely with ideal values. This study provides a solid alternative for liquefaction prediction, yielding more accurate findings than earlier research. Therefore, it can be said that this study introduces the SVM as a different and viable approach for classification tasks. The SVM has proven effective in evaluating liquefaction potential, incorporating mathematical functions. This work demonstrates the validity of SVM in modeling the complex relationships between seismic and soil parameters, as well as liquefaction potential, using in situ measurements based on the SPT.

#### FUNDING

This research received no external funding.

#### CONFLICTS OF INTEREST

The authors declare no conflict of interest.

#### AUTHORS CONTRIBUTION STATEMENT

Md. Mahabub Rahman, Md. Belal Hossain: conceptualization, formal analysis, writing – review & editing;

Md. Mahabub Rahman, Abu Sayed: methodology, roles/writing – original draft, visualization;

Md. Belal Hossain, Md. Mahabub Rahman: investigation, supervision;

Abu Sayed, Md. Mahabub Rahman: software;

Abu Sayed, Md. Belal Hossain: validation;

Abu Sayed: data curation.

#### REFERENCES

1. MORGENROTH J., ALMOND P., SCHARENBRUCH B.C., WILSON T.M., SHARP-HEWARD S., Soil profile inversion in earthquake-induced liquefaction-affected soils and the potential effects on urban trees, *Geoderma*, **213**: 155–162, 2014, <https://doi.org/10.1016/j.geoderma.2013.07.038>.
2. XUE X., YANG X., Seismic liquefaction potential assessed by support vector machines approaches, *Bulletin of Engineering Geology and the Environment*, **75**(1): 153–162, 2016, <https://doi.org/10.1007/s10064-015-0741-x>.

3. HAZOUT L., ZITOUNI Z.E.A., BELKHATIR M., SCHANZ T., Evaluation of static liquefaction characteristics of saturated loose sand through the mean grain size and extreme grain sizes, *Geotechnical and Geological Engineering*, **35**(5): 2079–2105, 2017, <https://doi.org/10.1007/s10706-017-0230-z>.
4. OBRADOVIC R., NAJDANOVIC N., *Mechanics of Soil in Engineering Practice*, Mining Institute, Belgrade, 1999.
5. AMBRASEYS N., BILHAM R., Reevaluated intensities for the great Assam earthquake of 12 June 1897, Shillong, India, *Bulletin of the Seismological Society of America*, **93**(2): 655–673, 2003, <https://doi.org/10.1785/0120020093>.
6. MOSTAZID M., RAHMAN M., RAHMAN M., Seismic vulnerability assessment of existing RCC buildings in Dinajpur City: a case study on ward no. 06, [in:] *Proceedings of International Conference on Planning, Architecture and Civil Engineering*, February 07–09, 2019.
7. BILHAM R., The seismic future of cities, *Bulletin of Earthquake Engineering*, **7**(4): 839–887, 2009, <https://doi.org/10.1007/s10518-009-9147-0>.
8. SEED H.B., IDRIS I.M., Simplified procedure for evaluating soil liquefaction potential, *Journal of the Soil Mechanics and Foundations Division*, **97**(9): 1249–1273, 1971, <https://doi.org/10.1061/JSFEAQ.0001662>.
9. BOULANGER R., IDRIS I., *CPT and SPT based liquefaction triggering procedures*, Report No. UCD/CGM-14/01, Center for Geotechnical Modeling, Department of Civil and Environmental Engineering, University of California, Davis, CA, 2014.
10. KAYEN R., MOSS R., THOMPSON E., SEED R., CETIN K., KIUREGHIAN A.D., TANAKA Y., TOKIMATSU K., Shear-wave velocity-based probabilistic and deterministic assessment of seismic soil liquefaction potential, *Journal of Geotechnical and Geoenvironmental Engineering*, **139**(3): 407–419, 2013, [https://doi.org/10.1061/\(ASCE\)GT.1943-5606.0000743](https://doi.org/10.1061/(ASCE)GT.1943-5606.0000743).
11. ZHANG W., WU C., ZHONG H., LI Y., WANG L., Prediction of undrained shear strength using extreme gradient boosting and random forest based on Bayesian optimization, *Geoscience Frontiers*, **12**(1): 469–477, 2021, <https://doi.org/10.1016/j.gsf.2020.03.007>.
12. PHAM B.T., NGUYEN M.D., BUI K.T.T., PRAKASH I., CHAPI K., BUI D.T., A novel artificial intelligence approach based on multi-layer perceptron neural network and biogeography-based optimization for predicting coefficient of consolidation of soil, *CATENA*, **173**: 302–311, 2019, <https://doi.org/10.1016/j.catena.2018.10.004>.
13. LE T.T., ASTERIS P.G., LEMONIS M.E., Prediction of axial load capacity of rectangular concrete-filled steel tube columns using machine learning techniques, *Engineering with Computers*, **38**(Supl 4): 3283–3316, 2021, <https://doi.org/10.1007/s00366-021-01461>.
14. LIN S., ZHENG H., HAN B., LI Y., HAN C., LI W., Comparative performance of eight ensemble learning approaches for the development of models of slope stability prediction, *Acta Geotechnica*, **17**(4): 1477–1502, 2022, <https://doi.org/10.1007/s11440-021-01440-1>.
15. NAJJAR Y.M., ALI H.E., CPT-based liquefaction potential assessment: A neuronet approach, [in:] *Geotechnical Earthquake Engineering and Soil Dynamics III*, pp. 542–553, ASCE, 1998.
16. KURUP P.U., GARG A., Evaluation of liquefaction potential using neural networks based on adaptive resonance theory, *Transportation Research Record*, **1936**(1): 192–200, 2005, <https://doi.org/10.1177/0361198105193600122>.

17. PAL M., Support vector machines-based modelling of seismic liquefaction potential, *International Journal for Numerical and Analytical Methods in Geomechanics*, **30**(10): 983–996, 2006, <https://doi.org/10.1002/nag.509>.
18. SAMUI P., Seismic liquefaction potential assessment by using Relevance Vector Machine, *Earthquake Engineering and Engineering Vibration*, **6**(4): 331–336, 2007, <https://doi.org/10.1007/s11803-007-0766-7>.
19. HANNA A.M., URAL D., SAYGILI G., Neural network model for liquefaction potential in soil deposits using Turkey and Taiwan earthquake data, *Soil Dynamics and Earthquake Engineering*, **27**(6): 521–540, 2007, <https://doi.org/10.1016/j.soildyn.2006.11.001>.
20. RAHMAN M.M., LO S.R., MOFIZ S.A., Artificial neural network in CPT base liquefaction prediction, [in] *17th Southeast Asian Geotechnical Conference, Taipei, Taiwan*, pp. 343–346, 2010.
21. KOHESTANI V.R., HASSANLOURAD M., ARDAKANI A.J.N.H., Evaluation of liquefaction potential based on CPT data using random forest, *Natural Hazards*, **79**(2): 1079–1089, 2015, <https://doi.org/10.1007/s11069-015-1893-5>.
22. ZHOU J., LI E., WANG M., CHEN X., SHI X., JIANG L., Feasibility of stochastic gradient boosting approach for evaluating seismic liquefaction potential based on SPT and CPT case histories, *Journal of Performance of Constructed Facilities*, **33**(3): 04019024, 2019, [https://doi.org/10.1061/\(ASCE\)CF.1943-5509.0001292](https://doi.org/10.1061/(ASCE)CF.1943-5509.0001292).
23. DAS S.K., MOHANTY R., MOHANTY M., MAHAMAYA M., Multi-objective feature selection (MOFS) algorithms for prediction of liquefaction susceptibility of soil based on in situ test methods, *Natural Hazards*, **103**: 2371–2393, 2020, <https://doi.org/10.1007/s11069-020-04089-3>.
24. AHMAD M., TANG X.W., QIU J.N., Application of machine learning algorithms for the evaluation of seismic soil liquefaction potential, *Frontiers of Structural and Civil Engineering*, **15**(2): 490–505, 2021, <https://doi.org/10.1007/s11709-020-0669-5>.
25. HU J., A new approach for constructing two Bayesian network models for predicting the liquefaction of gravelly soil, *Computer and Geotechnics*, **137**: 104304, 2021, <https://doi.org/10.1016/j.compgeo.2021.104304>.
26. HANANDEH S.M., AL-BODOUR W.A., HAJIJ M.M., A comparative study of soil liquefaction assessment using machine learning models, *Geotechnical and Geological Engineering*, **40**(9): 4721–4734, 2022, <https://doi.org/10.1007/s10706-022-02180-z>.
27. KUMAR D.R., SAMUI P., BURMAN A., WIPULANUSAT W., KEAWSAWASVONG S., Liquefaction susceptibility using machine learning based on SPT data, *Intelligent Systems with Applications*, **20**: 200281, 2023, <https://doi.org/10.1016/j.iswa.2023.200281>.
28. BHARDWAJ R.B., CHAURSIA S.R., Use of ANN, C4.5 and random forest algorithm in the evaluation of seismic soil liquefaction, *Journal of Soft Computing in Civil Engineering*, **6**(2): 94–113, 2022, <https://doi.org/10.22115/scce.2022.314762.1380>.
29. JANGIR H.K., SATAVALEKAR R., Evaluating adaptive neuro-fuzzy inference system (ANFIS) to assess liquefaction potential and settlements using CPT test data, *Journal of Soft Computing in Civil Engineering*, **6**(3): 119–139, 2022, <https://doi.org/10.22115/scce.2022.345237.1456>.
30. RAHMAN M.M., HOSSAIN M.B., SAYED A., THAKUR S., Assessment of liquefaction potential based on the logistic regression machine learning algorithm, *7th International Conference*

- 
- on Civil Engineering for Sustainable Development (ICCESD 2024)*, Bangladesh, 2024, <https://doi.org/10.13140/RG.2.2.24047.65440>.
31. HOSSAIN M.B., ROKNUZZAMAN M., RAHMAN M.M., Liquefaction potential evaluation by deterministic and probabilistic approaches, *Civil Engineering Journal*, **8**(7): 1459–1481, 2022, <https://doi.org/10.28991/CEJ-2022-08-07-010>.
  32. RAHMAN M.M., HOSSAIN M.B., ROKNUZZAMAN M., Effect of peak ground acceleration (PGA) on liquefaction behavior of subsoil: A case study of Dinajpur Sadar Upazila, Bangladesh, *AIP Conference Proceedings*, **2713**(1): 030002, 2023, <https://doi.org/10.1063/5.0129770>.
  33. SHI J.J., Clustering technique for evaluating and validating neural network performance, *Journal of Computing in Civil Engineering*, **16**(2): 152–155, 2002, [https://doi.org/10.1061/\(ASCE\)0887-3801\(2002\)16:2\(152\)](https://doi.org/10.1061/(ASCE)0887-3801(2002)16:2(152)).
  34. SHAHIN M.A., MAIER H.R., JAKSA M.B., Data division for developing neural networks applied to geotechnical engineering, *Journal of Computing in Civil Engineering*, **18**(2): 105–114, 2004, [https://doi.org/10.1061/\(ASCE\)0887-3801\(2004\)18:2\(105\)](https://doi.org/10.1061/(ASCE)0887-3801(2004)18:2(105)).
  35. DAS S.K., *Application of genetic algorithm and artificial neural network to some geotechnical engineering problems*, Ph.D Thesis, Department of Civil Engineering, IIT Kanpur (India), 2005.
  36. JIAN L., HUANG Z., ZHANG J., HU Z., Rapid analysis of cylindrical bypass flow field based on deep learning model, *IOP Conference Series: Earth and Environmental Science*, **1037**(1): 012013, 2022, <https://doi.org/10.1088/1755-1315/1037/1/012013>.
  37. SOKOLOVA M., LAPALME G., A systematic analysis of performance measures for classification tasks, *Information Processing & Management*, **45**(4): 427–437, 2009, <https://doi.org/10.1016/j.ipm.2009.03.002>.
  38. KRAEMER H.C., Kappa coefficient, [in:] *Wiley StatsRef: Statistics Reference Online*, Balakrishnan N., Colton T., Everitt B., Piegorisch W., Ruggeri F., Teugels J.L. [Eds.], 2014, <https://doi.org/10.1002/9781118445112.stat00365.pub2>.
  39. FAWCETT T., An introduction to ROC analysis, *Pattern Recognition Letters*, **27**(8): 861–874, 2006, <https://doi.org/10.1016/j.patrec.2005.10.010>.
  40. Scikit-Learn, *Receiver Operating Characteristic (ROC)*, (n.d.), [https://scikit-learn/stable/auto\\_examples/model\\_selection/plot\\_roc.html](https://scikit-learn/stable/auto_examples/model_selection/plot_roc.html) (accessed on 2024.01.04).

*Received May 6, 2024; accepted version March 25, 2025.*

*Online first May 27, 2025.*

---

